Drug Design, Development and Therapy

Dovepress
Taylor & Francis Group

Open Access Full Text Article

ORIGINAL RESEARCH

6-Hydroxygenistein Ameliorates High Altitude Brain Injury via Activating PI3K/AKT Signaling Pathway Based on Transcriptomic Analysis and Experimental Validation

Yu Xin[1,2], Gege Wang[2], Chenyu Yang[2], Huiping Ma[2], Linlin Jing[1,2]

[1]Department of Pharmacy, The First Affiliated Hospital of Xi'an Jiaotong University, Xi'an, Shaanxi, 710061, People's Republic of China; [2]Department of Pharmacy, The 940th Hospital of Joint Logistics Support Force of PLA, Lanzhou, Gansu, 730050, People's Republic of China

Correspondence: Linlin Jing, Department of Pharmacy, The First Affiliated Hospital of Xi'an Jiaotong University, No. 277 Yanta West Road, Yanta District, Xi'an, Shaanxi, 710061, People's Republic of China, Email jinglinlin@xjtufh.edu.cn; Huiping Ma, Department of pharmacy, The 940th Hospital of Joint Logistics Support force of PLA, No. 333 Binhe South Road, Qilihe District, Lanzhou, 730050, Gansu, People's Republic of China, Email huipingmacyk@163.com

Purpose: Our Prior research has shown that 6-hydroxygenistein (6-OHG) alleviates hypobaric hypoxia induced brain injury (HHBI) achieved by its powerful antioxidant, anti-inflammatory, and anti-apoptotic capabilities, but its mechanism still requires additional investigation. The objective of this study was to uncover the protective mechanism of 6-OHG against HHBI based on transcriptomics analysis and experimental validation.

Methods: The gene levels in brain tissue obtained from previous study were accessed via the RNA-Seq technique. DESeq2 R package was used to identify the differentially expressed genes (DEGs). Functional enrichment analysis and molecular docking were investigated utilizing the clusterProfiler R package and Autodock Vina software, respectively. In experimental validation stage, histological analysis was performed using Hematoxylin-Eosin (HE) staining. Oxidative stress, inflammatory, and apoptotic indexes in brain tissue were measured using commercial kits. Western blot was applied for detecting related protein expression.

Results: The RNA-Seq analysis revealed 905 differentially expressed genes (DEGs) between the Con and Mod groups, with 239 upregulated and 666 downregulated. Between the 6-OHG and Mod groups, there were 192 DEGs, including 98 upregulated and 94 downregulated genes. Go and KEGG function analyses highlighted the PI3K/AKT signaling pathway as a crucial regulatory mechanism. Western blot analysis showed that HH exposure caused a decrease in the ratios of p-PI3K/PI3K and p-AKT/AKT in the mouse brain, but this effect was reversed by 6-OHG treatment, indicating that 6-OHG activates the PI3K/AKT signaling pathway. Furthermore, LY294002, a selective PI3K inhibitor, effectively blocked this activation and also abolished the protective effects of 6-OHG on histopathological damage, as well as its antioxidant, anti-inflammatory, and anti-apoptotic activities in HHBI mice.

Conclusion: 6-OHG mitigates HHBI by activating the PI3K/AKT signaling pathway, suggesting its potential therapeutic application for HHBI treatment.

Keywords: 6-hydroxygenistein, transcriptomics, therapeutic target, hypobaric hypoxia induced brain damage, PI3K/AKT signaling pathway

Introduction

Areas above 2500 meters are called plateaus, which are characterized by hypobaric hypoxia (HH), cold temperatures, dry air, and strong solar radiation, making them one of the most challenging environments on Earth.[1] Among these factors, HH poses a particularly significant challenge. Exposure to HH environments lowers the partial pressure of inspired oxygen, which affects the lungs, brain, heart, and other organs, ultimately causing systemic damage.[2] The brain is one of the most oxygen-consuming organs in the mammalian body due to its high reliance on oxidative phosphorylation, which makes it very sensitive and vulnerable to hypoxia.[3] HH is capable of causing brain damage, which is mainly characteristic of morphological

Received: 30 March 2025
Accepted: 18 September 2025
Published: 23 September 2025

abnormalities, oxidative stress, mitochondrial dysfunction, inflammatory response, and apoptosis.[4] However, there is a lack of effective approaches for preventing and treating HH induced brain injury (HHBI), underscoring the urgent requirement for novel and effective therapeutic agents and strategies.

Transcriptomics, which examines gene expression at the RNA level, offers comprehensive insights into gene structure and function, enabling the elucidation of molecular mechanisms underlying specific biological processes.[5] In recent years, RNA sequencing (RNA-seq) combined with bioinformatics analysis has been widely employed to identify the molecular mechanisms of drugs utilized for preventing and treating high-altitude-related tissue damage.[6,7]

4′,5,6,7-tetrahydroxyisoflavone (6-hydroxygenistein, 6-OHG, Figure 1), an active ingredient in fermented soybean foods,[8] possesses some health-related biological roles such as hepatoprotective,[9] anti-hypoxia,[10] anticancer,[11] and antimelanogenesis[12] activities. Recently, our research demonstrated that 6-OHG mitigates HHBI by activating the Nrf2/HO-1 pathway and inhibiting the NF-κB/NLRP3 pathway.[13] However, the precise regulatory mechanisms by which 6-OHG modulates these pathways remain to be fully elucidated. In this study, a mice model of HHBI was employed to investigate the protective mechanism of 6-OHG via transcriptomics analysis and experimental validation.

Materials and Methods

Reagents

6-OHG was synthesized following the procedure we previously described.[14] The Bicinchoninic Acid (BCA) protein assay kit (PC0020) was provided by Beijing Solarbio Science & Technology Co., Ltd (Beijing, China). The kits of hydrogen peroxide (H_2O_2, A064-1-1), glutathione (GSH, A006-2-1), malondialdehyde (MDA, A003-1-2), superoxide Dismutase (SOD, A001-3-2), Caspase-3 (G015-1-2), and Caspase-9 (G018-1-2) were provided by Nanjing Jiancheng Bioengineering Institute (Nanjing, China). Mouse tumor necrosis factor-α (TNF-α, RX202412M), interleukin-1β (IL-1β, RX203063M), interleukin-6 (IL-6, RX203049M), and interleukin-10 (IL-10, RX203075M) ELISA kits were provided by Quanzhou Ruixin BioTechnology Co., LTD (Quanzhou, China). The primary antibodies against *β*-actin (ab8227) were purchased from Abcam (Cambridge, UK). The primary antibodies against PI3K (4292S), p-PI3K (4228S), AKT (9272S), and p-AKT (4060S) were purchased from Cell Signaling Technology (Danvers, USA). The primary antibodies against Bax (50599-2-lg) and Bcl-2 (AF6139) were obtained from Proteintech (Wuhan, China) and Affinity (Jiangsu, China), respectively. Goat anti-mouse IgG and Goat anti-rabbit IgG were obtained from Zhongshan Golden Bridge Biological Technology Co., Ltd. (Beijing, China).

Animal

Male Balb/c mice (age: 7 weeks, weight: 20 ± 2 g) were obtained from the Laboratory Animal Center of the Air Force Medical University (Xian, China). The mice were housed under controlled conditions (23–25 °C, 12-hour light/dark cycle) with ad libitum to food and water. Animal experiments were approved by the Animal Care and Use Committee of 940th Hospital (No: 2021KYLL241) and were conducted in strict accordance with the National Research Council's Guide for the Care and Use of Laboratory Animals. The utilization of experimental animals and their associated discomfort were significantly minimized. Mice were acclimatized for one week before the start of experiment.

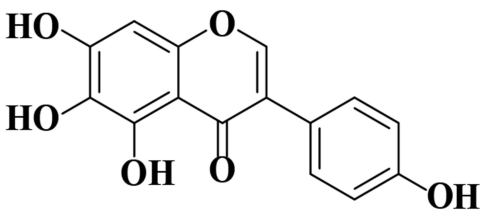

Figure 1 Chemical structure of 6-OHG.

Establishment of HHBI Model

The HHBI model was established as reported previously.[13] Briefly, eighteen mice were randomly classified into three groups (n = 6 per group): control (Con) group, hypobaric hypoxia (Mod) group, and HH plus 6-OHG (6-OHG) group. Mice in the Con and Mod groups were intraperitoneally injected with saline, while mice in the 6-OHG group were intraperitoneally injected with 6-OHG (100 mg/kg, suspended in 5% Tween 80 in saline). After 30 min, the mice in the Con group were housed under normal conditions, whereas the mice in Mod and 6-OHG groups were placed in an animal decompression chamber (DYC-3070, Guizhou Fenglei, China) and subjected to a mimic height of 8000 m (0.035 MPa, humidity, 40–50%, and temperature, 23–25 °C) for 24 h. Although the oxygen fraction remained near 21%, the reduced atmospheric pressure resulted in a markedly lower partial pressure of oxygen (PO_2), thereby inducing severe hypoxic conditions. Mice were *ad libitum* access to food and water during the experimental period. After 24 h, the mice were euthanized. The brain tissue was collected for transcriptomic assays.

We further examined the underlying mechanisms in the next study period. Forty mice were randomly classified into four groups (n = 10 per group): Con group, HHBI group, HHBI+6-OHG, and HHBI+6-OHG plus PI3K inhibitor LY294002[15] (HHBI+6-OHG+LY) group. For the HHBI+6-OHG+LY group, LY294002 (10 mg/kg, dissolved in 10% DMSO-saline solution, with the dose determined based on our previous study[16]) was intraperitoneally injected into the mice 30 min before 6-OHG administration. Other protocols were identical to those described above.

Total RNA Extraction and Transcriptome Sequencing Analysis

The RNA-seq analysis was carried out by Biotree Biotech Co., Ltd. (Shanghai, China). Total RNA was extracted from brain tissue using the Trizol reagent (thermofisher, 15596018). A total of 13 RNA samples (four samples in both the Con and the 6-OHG groups, and five samples in the Mod group) were obtained. Bioanalyzer 2100 and NanoDrop 2000 Spectrophotometer (Thermo Scientific, USA) was utilized to analyze RNA quantity and purity. The RNA-seq library preparation was then performed utilizing NEBNext® UltraTM RNA Library Prep Kit for Illumina® (NEB, USA). The library was sequenced on an illumina Novaseq 6000 platform, producing 150 bp paired-end reads. Low-quality reads were removed using Cutadapt and clean reads were aligned to the mouse reference genome (mm10) using HISAT2. The expression levels of all transcripts were estimated using StringTie, with mRNA abundance quantified in FPKM (fragments per kilobase of transcript per million mapped reads). Differentially expressed genes (DEGs) between two groups were identified using DESeq2 ($|\log2FoldChange| \geq 1$, adjusted p-values (padj < 0.05)). Principal components analysis (PCA), Gene Ontology (GO) and Kyoto Encyclopedia of Genes and Genomes (KEGG) enrichment analyses were conducted utilizing the clusterProfiler R package.

Histopathological Analysis

From each group, three mouse brain tissue specimens were randomly selected. Brain tissues were isolated and soaked in paraformaldehyde (4%). Then tissues were embedded in paraffin wax and cut into 5 μm thick sections using a microtome. The slices were dewaxed using xylene and hydrated with ethanol. After rinsing with distilled water, it was stained with hematoxylin and eosin (H&E). Gradient dehydration was performed using 75%, 85%, 95%, and 100% ethanol. Finally, the slices were observed and photographed using a Pannoramic MIDI II Digital Scanner (3DHISTECH Ltd., Budapest, Hungary) equipped with a 40x objective lens (numerical aperture, NA = 0.95). For analysis and presentation, 40x magnification images were utilized. Subsequently, semiquantitative assessment was employed to evaluate alterations in brain tissue pathology based on the following parameters: severity of edema (0–3 points), degree of vascular congestion (0–3 points), and extent of neuronal damage (0–3 points). Each parameter was scored independently, and a total neuropathology score (ranging from 0 to 9) was calculated for each region.

Biochemical Analysis

From each group, six mouse brain tissue specimens were randomly selected for the quantification of H_2O_2, MDA, GSH, SOD, caspase-3, and −9 using corresponding commercial kits (Nanjing Jiancheng Bioengineering Institute, Nanjing, China).

ELISA Analysis

From each group, six mouse brain tissue specimens were randomly selected, and the concentrations of inflammatory factors, including TNF-α, IL-1β, IL-6, and IL-10 were assessed using corresponding commercial ELISA kits (Quanzhou Ruixin BioTechnology Co., LTD, Quanzhou, China).

Western Blotting Analysis

From each group, five mouse brain tissue specimens were randomly selected. The brain tissue was lysed in RIPA buffer supplemented with protease inhibitor and phosphatase inhibitor. Protein contents were quantified by the BCA assay kit. Tissue lysates were loaded onto Sodium dodecyl sulfate-polyacrylamide gel electrophoresis (SDS-PAGE), and then transferred to the PVDF membranes (Millipore, USA). After blocking with 5% (w/v) skimmed milk in TBST buffer, the membranes were incubated with primary antibodies at 4 °C overnight, and subsequently incubated with HRP-conjugated secondary antibodies for 120 min at 25 °C. The bands were visualized by enhanced chemiluminescence (ECL) reagent and recorded on ChemiDoc MP imaging system (Hercules, CA, USA). β-actin was employed as an endogenous loading control to ensure equal protein loading in each lane. ImageJ software was employed to quantify the band intensity.

Molecular Docking

The crystal structures of PI3K (PDB ID: 4JPS) and AKT (PDB ID: 8UW9) proteins were obtained from RCSB protein data bank (https://www.rcsb.org/). Water molecules, salt ions, and other small molecules in proteins were removed using PyMOL software (version 3.0.0). The 3D structure of 6-OHG (compound CID: 6063386) was obtained from PubChem (https://pubchem.ncbi.nlm.nih.gov/). Using AutoDock Tools (version 1.5.7), the protein structures were prepared by adding hydrogen atoms, calculating atomic charges, and merging nonpolar hydrogens. The small molecule ligand (6-OHG) was prepared through hydrogenation and bond flexibility assignment. The docking search space was defined using a grid box with the following parameters: for PI3K, the center was set at (X, Y, Z) = (−37.5, −15.6, 27.8) with dimensions (X × Y × Z) = 25 × 25×25 Å, located within the p85α-nSH2-adjacent region; for AKT1, the center was set at (25, 12, −28) with dimensions of 20 × 20×20 Å, situated at the PH-kinase interface within the allosteric pocket. An exhaustiveness value of 32 was used for the docking calculations. Molecular docking of 6-OHG with each protein was performed using AutoDock Vina (version 1.2.7). The resulting docking poses were visualized and analyzed using PyMOL and Discovery Studio (version 4.5).

Statistical Analysis

Investigators involved in data collection and analysis were blinded to the group allocation during the experiment and assessment. Data were presented as mean ± standard deviation (SD). Statistical analysis was performed utilizing GraphPad Prism 8.0 software. One-way analysis of variance (ANOVA) with Tukey's test was performed for the comparison between groups. A *P*-value of less than 0.05 was regarded as statistically significant.

Results

Transcriptome Profiling of Brain Tissue

As shown in Table S1, the Q30 base distribution ranged from 97.22% to 97.98%, indicating trustworthy sequencing data suitable for downstream analysis. Clean reads were mapped to the mouse reference genome (mm10) with mapping ratios between 95.57% and 96.87% (Table S2). Gene expression levels were quantified using RPKM values. Boxplots illustrating the distribution of gene expression across all 13 datasets were presented in Figure 2A. Density plots revealed similar gene expression distribution patterns across the 13 samples in the three groups (Figure 2B). Pearson's correlation coefficients between biological replicates exceeded 0.99, demonstrating high reproducibility of the sequencing results (Figure 2C). These resulting indicated that the sequencing data met the requirements for further analysis. PCA showed independent separation among the three groups in the principal component of the PC1×PC2 score plot (Figure 2D). The heat-map among the three groups showed significantly changed genes (Figure 2E).

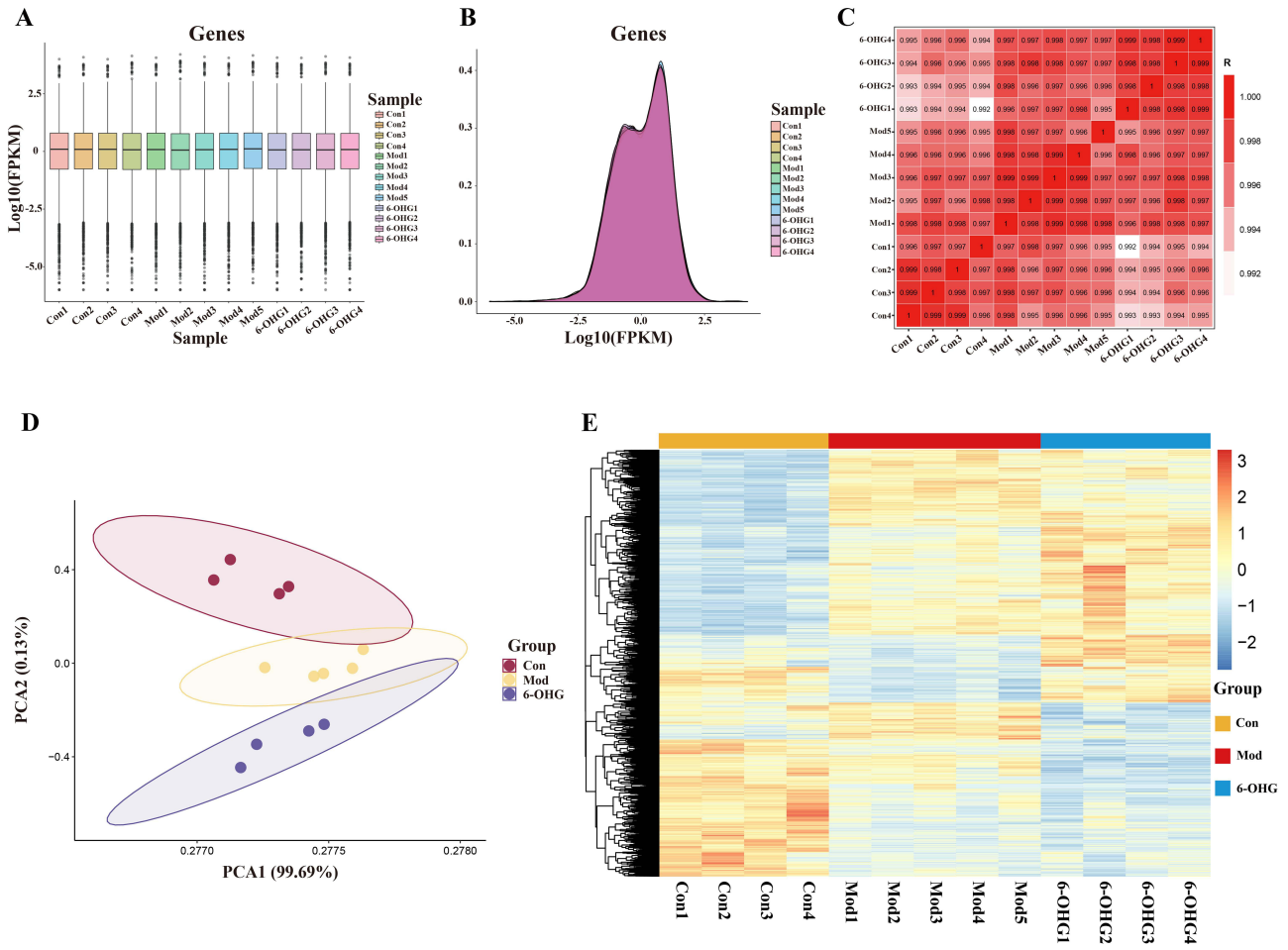

Figure 2 Features of sequencing data. (**A**) Box plot of log2 (RPKM) expression values for each sample. (**B**) Density plot of the distribution of log2 (RPKM) values for each sample. (**C**) Pearson's correlation analysis between samples. (**D**) PCA analysis. (**E**) Hierarchical clustering heatmap of the DEGs.

DEGs Analysis

As shown in Figure 3A–D, 905 DEGs (239 upregulated and 666 downregulated) in the Con vs Mod groups, and 192 DEGs (98 upregulated and 94 downregulated) in the 6-OHG vs Mod groups were found. Meanwhile, 10 DEGs overlapped between the Con vs Mod groups and the 6-OHG vs Mod groups (Figure 3E).

Enrichment Analysis of DEGs

GO functional enrichment analysis was performed to annotate gene functions and categorize the DEGs into biological process (BP), cellular component (CC), and molecular function (MF) (Figure 4A and B). In the BP module, the DEGs in the Con vs Mod groups were primarily enriched in signal transduction, biological process, multicellular organism development, cell differentiation, positive regulation of transcription by RNA polymerase II, and apoptotic process; while the DEGs in the 6-OHG vs Mod groups were primarily enriched in positive regulation of transcription by RNA polymerase II, biological process, regulation of DNA-templated transcription, signal transduction, and innate immune response. In the CC module, DEGs both in the Con vs Mod groups and 6-OHG vs Mod groups were primarily enriched in the membrane, cytoplasm, nucleus, and plasma membrane. In the MF module, protein binding, metal ion binding, molecular function, DNA binding, and nucleotide binding were significantly enriched in both Con vs Mod groups and 6-OHG vs Mod groups.

KEGG pathway enrichment analysis for these DEGs in the Con vs Mod and 6-OHG vs Mod groups was performed separately (Figure 4C and D). We found that the PI3K/AKT pathway, neuroactive ligand-receptor interaction, Ras pathway, and MAPK pathway, were remarkably enriched for the DEGs in both Con vs Mod groups and 6-OHG vs Mod groups. We

https://doi.org/10.2147/DDDT.S526988

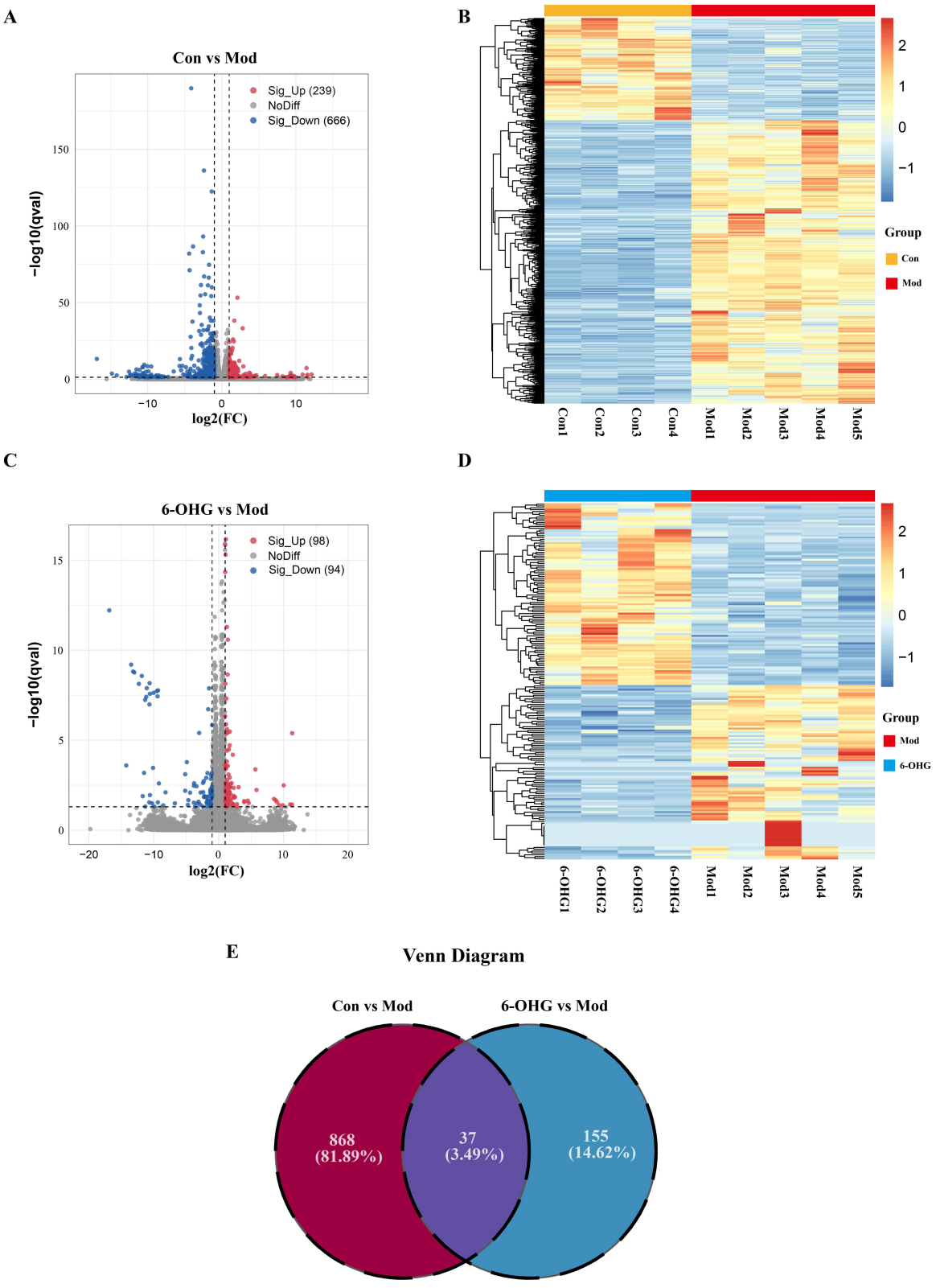

Figure 3 Analysis of DEGs. (**A**) Volcano map of DEGs in the Con vs Mod groups. (**B**) Volcano map of DEGs in the 6-OHG vs Mod groups. (**C**) Hierarchical clustering heatmap of DEGs in the Con vs Mod groups. (**D**) Hierarchical clustering heatmap of DEGs in the 6-OHG vs Mod groups. (**E**) Venn Diagram of overlapping DEGs.

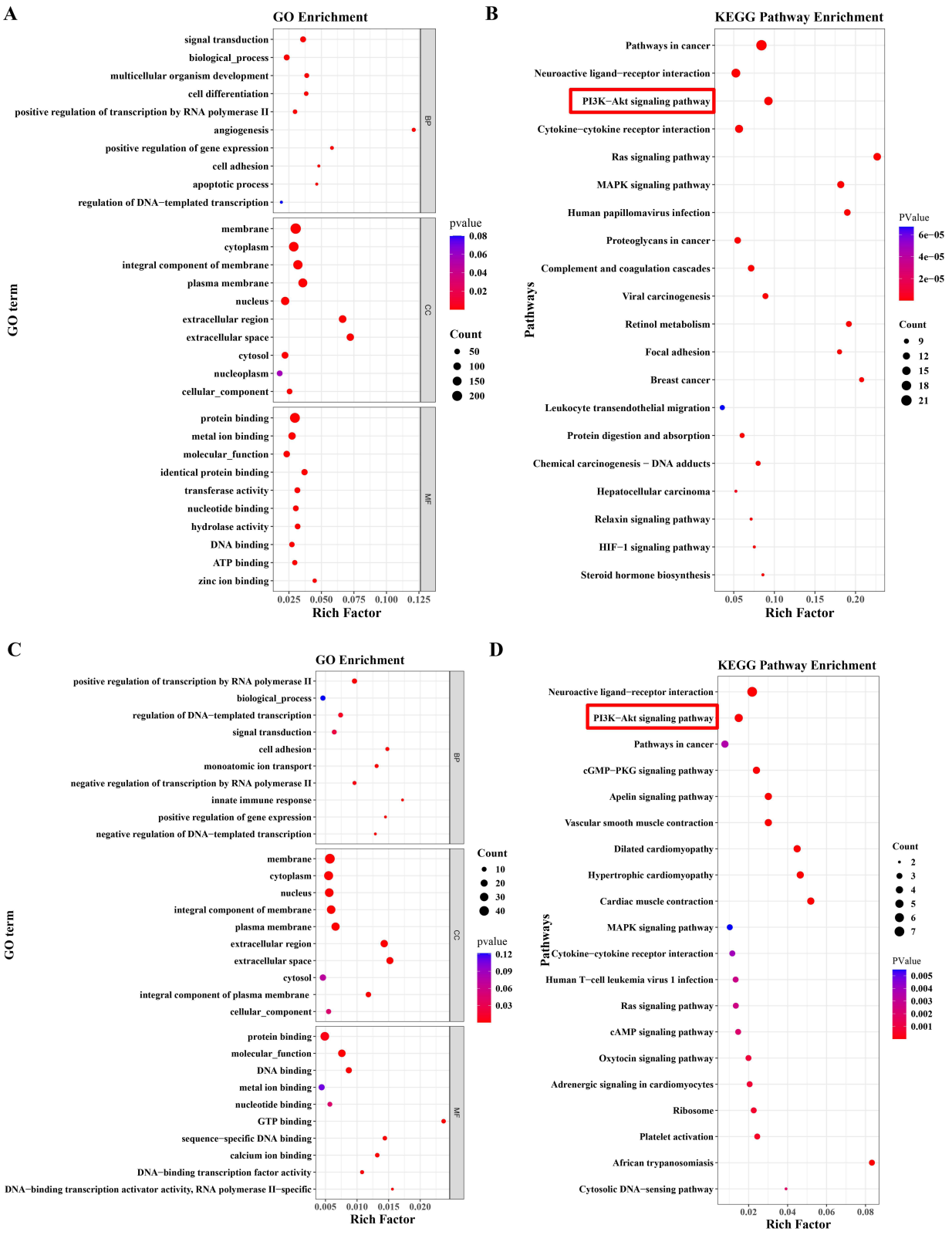

Figure 4 Bioinformatic analysis. (**A**) GO enrichment analysis of DEGs in the Con vs Mod groups. (**B**) GO enrichment analysis of DEGs in the 6-OHG vs Mod groups. The top 10 significantly enriched categories were shown. (**C**) KEGG enrichment analysis of DEGs in the Con vs Mod groups. (**D**) KEGG enrichment analysis of DEGs in the 6-OHG vs Mod groups. The top 20 significantly enriched pathways were shown.

https://doi.org/10.2147/DDDT.S526988

proposed that the PI3K/AKT signaling pathway potentially serves as a crucial mechanism underlying 6-OHG-mediated neuroprotection against HHBI.

Screening for DEGs Related to PI3K/AKT Signaling Pathway

To better capture the changes of PI3K/AKT signaling pathway-related genes, the heatmaps were constructed to give a pictorial view. Compared to Con group, HH exposure significantly decreased the levels of Igf2, Tnc, and Bdnf, significantly increased the levels of Angpt2, Vegfa, Col4a1, Flt4, Cdkn1a, Epha2, Pgf, Il2rg, Col2a1, Tnn, and Epo (Figure 5A). Compared to Mod group, 6-OHG treatment markedly decreased the levels of Pgf, Gng11, Il3ra, and Efna4, whereas markedly enhanced the level of Nr4a1 (Figure 5B).

LY294002 Offset the Activation of PI3K/AKT Signaling Pathway by 6-OHG

Bioinformatics analysis indicated that the PI3K/AKT signaling pathway plays a role in the protective effect of 6-OHG against HHBI. To further confirm this finding, Western blot was employed to analyze PI3K/AKT signaling pathway-related proteins, such as PI3K, p-PI3K, AKT, and p-AKT. As shown in Figure 6A–C and Figure S1, HH exposure significantly reduced the p-PI3K/PI3K and p-AKT/AKT ratios in brain tissue by 60% (95% CI: 49% to 70%) and 52% (95% CI: 30% to 65%), respectively, compared to the control group (both $P < 0.01$). Treatment with 6-OHG effectively reversed these changes, increasing the p-PI3K/PI3K and p-AKT/AKT ratios by 2.09-fold (95% CI: 1.53 to 2.86, $P < 0.01$) and 1.70-fold (95% CI: 1.19 to 2.36, $P < 0.05$), respectively, compared to the HHBI group. Notably, the specific PI3K inhibitor LY294002 abolished the effects of 6-OHG. In the LY294002-treated group, the p-PI3K/PI3K and p-AKT/AKT ratios decreased by 67% (95% CI: 54% to 78%, $P < 0.01$) and 47% (95% CI: 23% to 63%, $P < 0.05$), respectively, compared to the 6-OHG group, confirming that the effects of 6-OHG are mediated through the PI3K/AKT pathway.

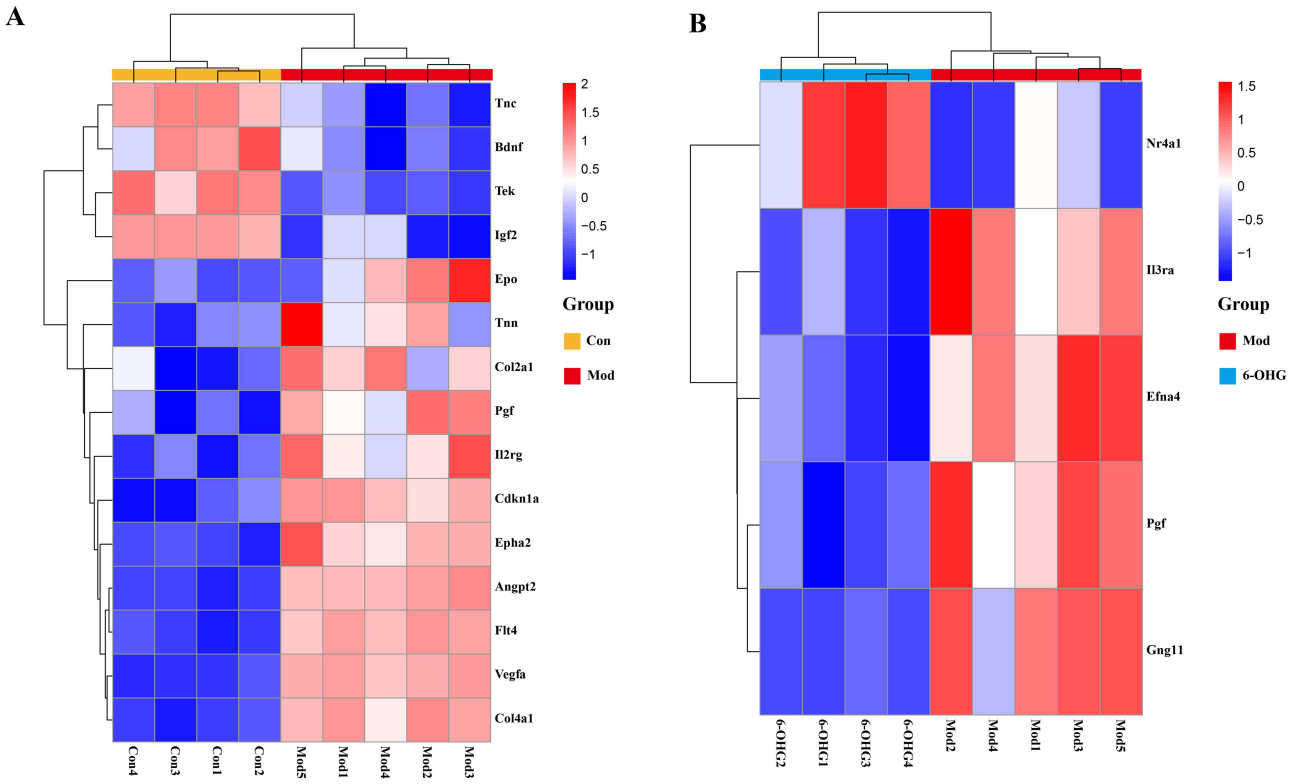

Figure 5 Effect of 6-OHG on the PI3K/AKT signaling pathway following HH exposure. (**A**) Hierarchical clustering heatmap of the DEGs related to PI3K/AKT signaling pathway in the Con vs Mod groups (**B**) Hierarchical clustering heatmap of the DEGs related to PI3K/AKT signaling pathway in 6-OHG vs Mod groups.

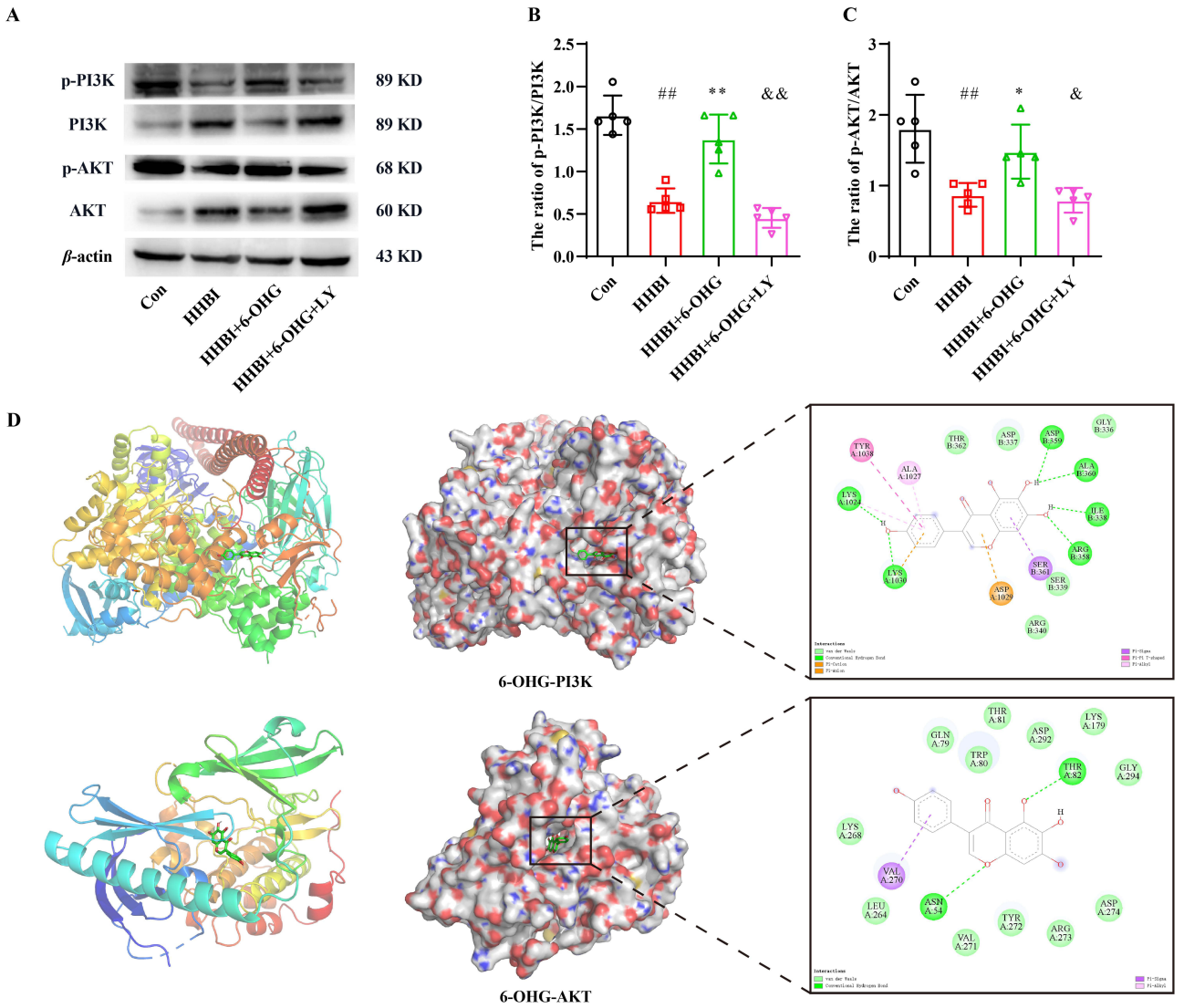

Figure 6 LY294002 offset the activation of PI3K/AKT signaling pathway by 6-OHG. (**A**) Representative Western blots of p-PI3K, PI3K, p-AKT, and AKT in brain tissue. (**B**) Quantitative analysis of the p-PI3K/PI3K ratio in brain tissue. (**C**) Quantitative analysis of the p-AKT/AKT ratio in brain tissue. Data are presented as mean ± SD. n =5 per group, $^{\#\#}P$ <0.01 vs Con group. $^{*}P$ <0.05, $^{**}P$ <0.01 vs HHBI group. $^{\&}P$ <0.05, $^{\&\&}P$ <0.01 vs HHBI + 6-OHG group. (**D**) Visualization of the docking results of 6-OHG binding to PI3K and AKT.

Molecular Docking Analysis

To elucidate the interaction mode of 6-OHG with PI3K/Akt pathway, the potential target amino acid residues and intermolecular interactions of 6-OHG with PI3K and AKT were also predicted using molecular docking. As shown in Figure 6D and Table 1, 6-OHG was able to enter the active pocket of both proteins, with binding free energies of −8.00 kcal/mol for PI3K and −9.12 kcal/mol for AKT, respectively. All the optimal conformations exhibited cluster RMSDs of 0 Å and formed at least two hydrogen bonds. Additionally, interactions such as van der Waals forces, Pi-Anion, Pi-Sigma, Amide-

Table 1 Autodock Scores and Stability Evaluation of Optimal Docking Conformations

Ligands	Receptors	Free Energy of Binding	Cluster RMSD	Hydrogen Bond Sites
6-OHG	PI3K (4JPS)	−8.00 kcal/mol	0 Å	A: LYS-1024, LYS-1030 B: ILE-338, ARG-358, ASP-359, ALA-360
6-OHG	AKT (8UW9)	−9.12 kcal/mol	0 Å	THR-82, ASN-54

https://doi.org/10.2147/DDDT.S526988

Pi, Pi-Alkyl, Pi-Pi T-shaped, and Pi-Sulfur were identified, which may contribute to the stability of 6-OHG binding to PI3K and AKT. These findings demonstrate that 6-OHG may regulate the PI3K/AKT signaling pathway through direct interactions with these proteins.

LY294002 Attenuated the Neuroprotective Efficacy of 6-OHG Against HH-Induced Histopathological Damage in Mice Brain

The histopathological changes were accessed by H&E staining. As shown in Figure 7A and B, HH exposure resulted in structural and functional abnormalities in neurons, evidenced by disorderly arranged and edema neurons, and dilated blood vessels. These changes were ameliorated by 6-OHG treatment. However, the beneficial effects of 6-OHG were attenuated by LY294002, indicating that the neuroprotective effects of 6-OHG are mediated through the PI3K/AKT pathway.

LY294002 Counteracted the Anti-Oxidant Stress Effect of 6-OHG

As seen in Figure 8A–D, compared to the control group, HH exposure markedly elevated H_2O_2 and MDA levels in brain tissue by 1.93-fold (95% CI: 1.57 to 2.41) and 2.29-fold (95% CI: 2.02 to 2.57), respectively, and reduced SOD activity and GSH content to 70% (95% CI: 62% to 78%) and 54% (95% CI: 43% to 68%), respectively (all $P < 0.01$). Treatment with 6-OHG significantly reversed these HH-induced changes, decreasing H_2O_2 and MDA contents by 39% (95% CI: 36% to 40%) and 33% (95% CI: 27% to 45%), and increasing SOD activity and GSH content by 1.24-fold (95% CI: 1.12 to1.36) and 1.51-fold (95% CI: 1.22 to1.89), respectively, compared to the HHBI group (all $P < 0.01$). Notably, LY294002 abolished the effects of 6-OHG. In the LY294002-treated groups, H_2O_2 and MDA contents increased by 1.37-fold (95% CI: 1.15 to 1.62, $P < 0.01$) and 1.30-fold (95% CI: 1.07 to 1.57, $P < 0.05$), whereas SOD activity and GSH content decreased by 15% (95% CI: 6% to 23%, $P < 0.05$) and 29% (95% CI: 14% to 43%, $P < 0.05$), respectively, compared to the 6-OHG group. These results suggest hat the antioxidant effects of 6-OHG are mediated through the PI3K/AKT pathway.

LY294002 Counteracted the Anti-Inflammatory Role of 6-OHG

As seen in Figure 8E–H, compared to the control group, HH exposure markedly elevated the concentrations of pro-inflammatory factors in brain tissue, including TNF-α, IL-1β, and IL-6, by 1.49-fold (95% CI: 1.31 to 1.69), 1.42-fold

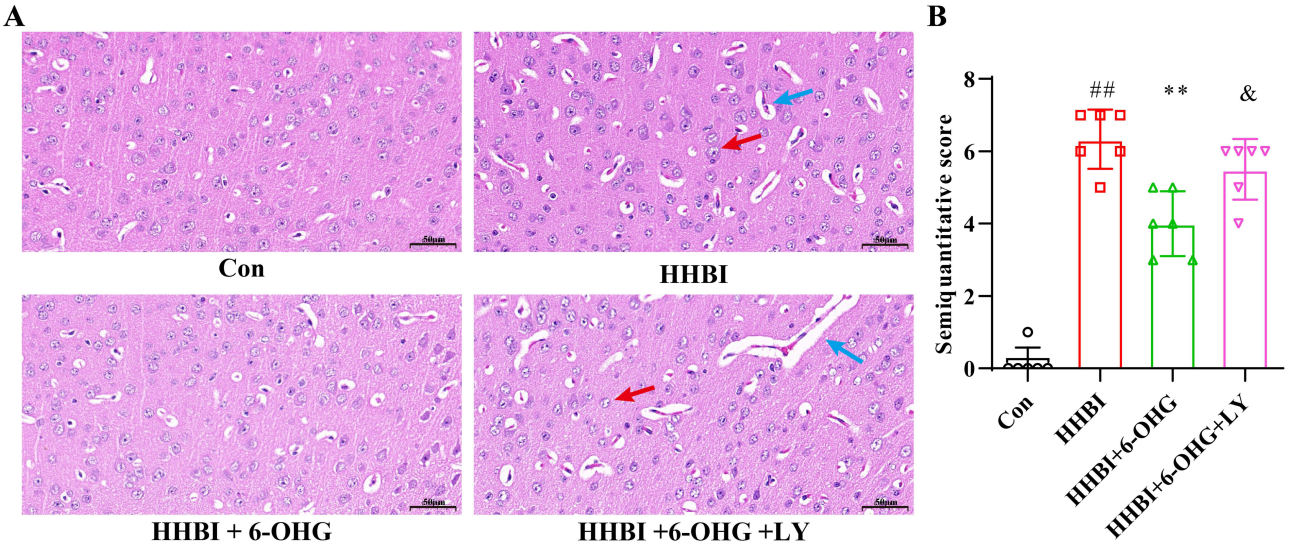

Figure 7 LY294002 reversed the protective effect of 6-OHG on HH-induced histopathological damage in mice brain. (**A**) Representative images of H&E staining in the cortex (40× magnification, scale bar = 50 μm). Red arrows indicated cell edema. Blue arrows indicated dilation of blood vessel congestive. (**B**) Semiquantitative Score of Brain Histopathological Injury. Data are presented as the mean ± SD. n = 3 mice/group, two images per mouse. $^{\#\#}P$ <0.01 vs Con group. $^{**}P$ <0.01 vs HHBI group. $^{\&}P$ <0.05 vs HHBI + 6-OHG group.

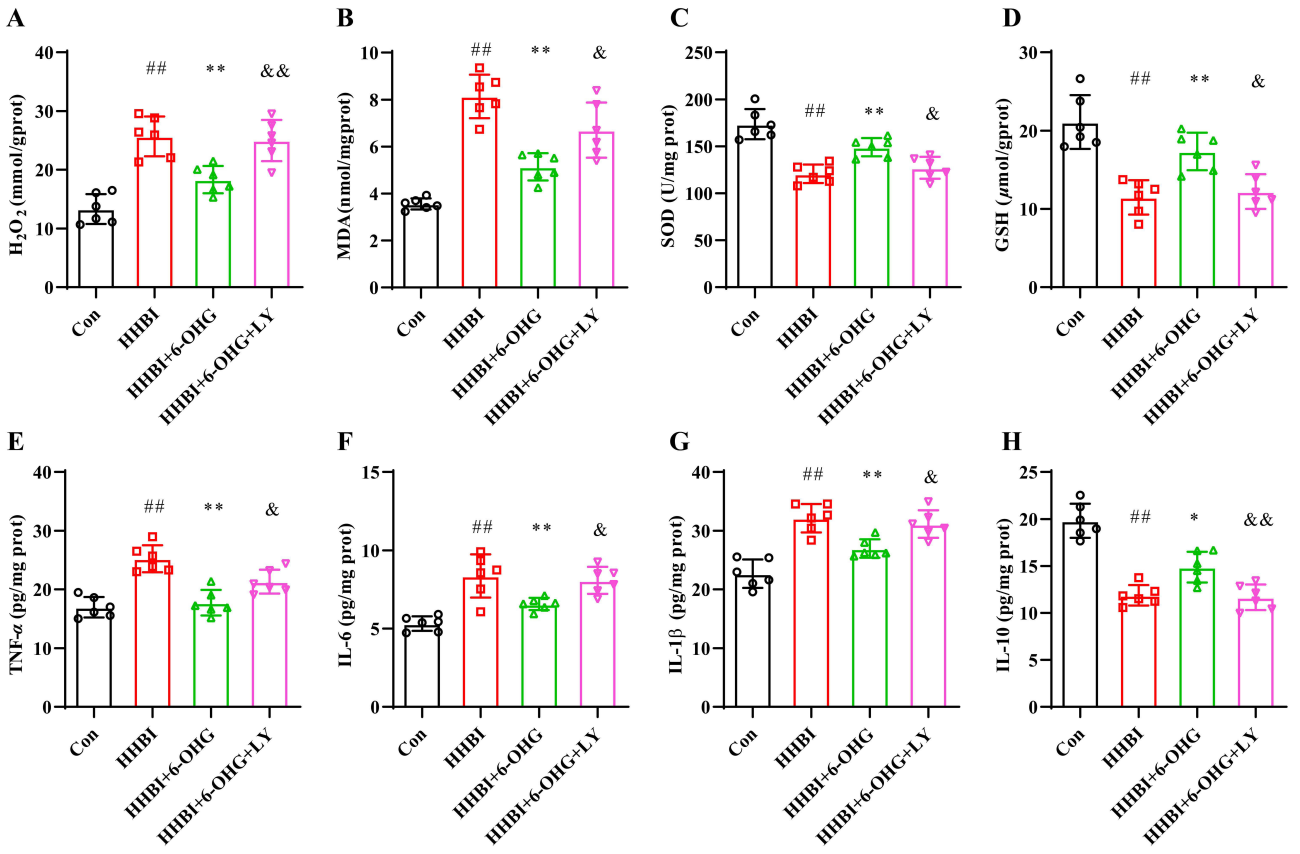

Figure 8 LY294002 counteracted the anti-oxidant stress and anti-inflammatory roles of 6-OHG. (**A**) H_2O_2 content. (**B**) MDA content. (**C**) SOD activity. (**D**) GSH content. (**E**) TNF-α content. (**F**) IL-6 content. (**G**) IL-1β content. (**H**) IL-10 content. Data are presented as mean ± SD. n =6 per group. $^{\#\#}P$ <0.01 vs Con group. $^{*}P$ <0.05, $^{**}P$ <0.01 vs HHBI group. $^{\&}P$ <0.05, $^{\&\&}P$ <0.01 vs HHBI + 6-OHG group.

(95% CI: 1.26 to 1.60), and 1.57-fold (95% CI: 1.31 to 1.85), respectively, and reduced the level of anti-inflammatory factor (IL-10) to 60% (95% CI: 53% to 67%) (all $P < 0.01$). Treatment with 6-OHG inhibited inflammatory response by decreasing the release of TNF-α, IL-1β, and IL-6 by 30% (95% CI: 19% to 39%), 16% (95% CI: 8% to 23%), and 21% (95% CI: 7% to 32%), respectively (all $P < 0.01$), and increasing IL-10 level by 1.25-fold (95% CI: 1.10 to 1.43, $P < 0.05$), compared to the HHBI group. These beneficial effects were reversed by LY294002. In the LY294002-treated groups, the levels of TNF-α, IL-1β, and IL-6 increased by 1.20-fold (95% CI: 1.01 to 1.39), 1.15-fold (95% CI: 1.06 to 1.26), and 1.23-fold (95% CI: 1.10 to 1.37), respectively (all $P < 0.05$), whereas IL-10 level decreased by 21% (95% CI: 9% to 32%, $P < 0.01$), compared to the 6-OHG group. These results indicate that the anti-inflammatory properties of 6-OHG depend on PI3K/AKT pathway activation.

LY294002 Counteracted the Anti-Apoptotic Role of 6-OHG

The PI3K/AKT pathway is crucial in regulating apoptosis. Therefore, we investigated the activities of Caspase-3 and −9, and the expression of Bax and Bcl-2 in the brain tissue. As shown in Figure 9A–D and Figure S2 HH exposure significantly increased caspase-3 activity by 1.86-fold (95% CI: 1.55 to 2.25), caspase-9 activity by 2.24-fold (95% CI: 1.94 to 2.60), and the Bax/Bcl-2 ratio by 1.57-fold (95% CI: 1.25 to 1.94) compared to the control group (all $P < 0.01$). Treatment with 6-OHG reversed these effects, decreasing caspase-3 activity, caspase-9 activity, and Bax/Bcl-2 ratio by 27% (95% CI: 13% to 39%), 39% (95% CI: 24% to 53%), and 33% (95% CI: 19% to 44%), respectively, compared to the HHBI group (all $P < 0.01$). However, the anti-apoptotic effects of 6-OHG were counteracted by LY294002. In the LY294002-treated groups, caspase-3 activity, caspase-9 activity, and the Bax/Bcl-2 ratio increased by 1.25-fold (95% CI: 1.07 to 1.49, $P < 0.05$), 1.29-fold (95% CI: 1.04 to 1.69, $P < 0.05$), and 1.55-fold (95% CI: 1.36 to 1.79, $P < 0.01$),

https://doi.org/10.2147/DDDT.S526988

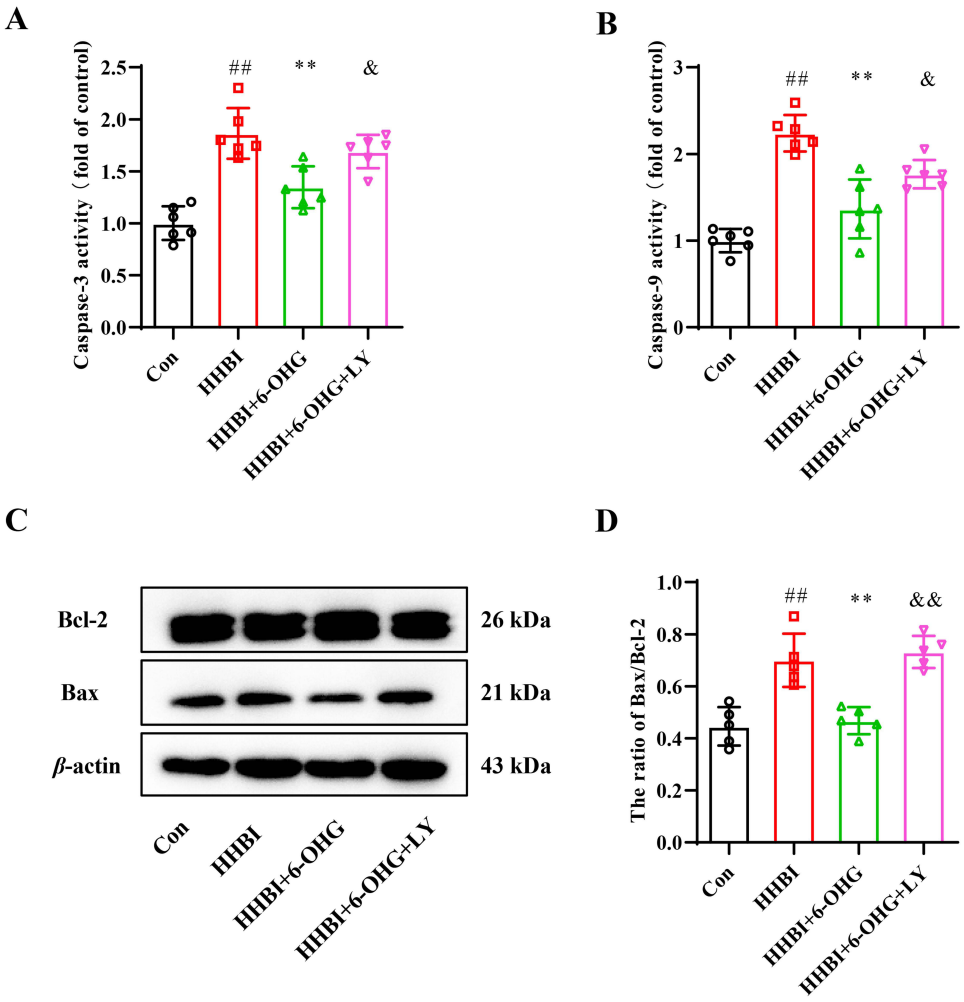

Figure 9 LY294002 counteracted the anti-apoptosis effect of 6-OHG. (**A**) Caspase-3 activity. (**B**) Caspase-9 activity. (**C**) Representative Western blots of Bax and Bcl-2 in brain tissue. (**D**) Quantitative analysis of the Bax/Bcl-2 ratio in brain tissue. Data are presented as mean ± SD. n =5 or 6 per group. $^{\#\#}P$ <0.01 vs Con group. $^{**}P$ <0.01 vs HHBI group. $^{\&}P$ <0.05, $^{\&\&}P$ <0.01 vs HHBI + 6-OHG group.

respectively, compared to the 6-OHG group. These results suggest that 6-OHG suppresses HH-induced neuronal apoptosis, partially by activating the PI3K/AKT signaling pathway.

Discussion

HHBI is a common central nervous system (CNS) disorder encountered at high altitude. Despite its significant impact on health, the underlying mechanisms of HHBI are still poorly understood, and current therapeutic strategies in clinical practice are very limited. 6-OHG is a natural flavonoid, that owns anti-inflammatory, antioxidant, and anti-apoptotic activities and exerts potential neuroprotective effects on HHBI.[13] To further elucidate the mechanism by which 6-OHG protects against HHBI and to establish a scientific foundation for its potential clinical application, this study systematically identified the key pathways through transcriptomics and animal experiments. The present findings provided substantial evidence that 6-OHG treatment alleviated HHBI by suppressing oxidative stress, neuroinflammation, and apoptosis via activating the PI3K/AKT signaling pathways.

The PI3K/AKT pathway, which is responsible for the survival, differentiation, proliferation, apoptosis, and metabolism of neurons, is essential in the brain.[17] Its activation is critical for neuroprotection and neuronal survival,[18] while its inhibition contributes to the pathogenesis of HH induced injury, such as cerebral edema,[19] lung injury,[20] myocardial injury[21] and pulmonary hypertension.[22] In our previous study, we found that 6-OHG treatment conversed HH induced damage to the brain.[13] In the current study, a transcriptome analysis was conducted and the results hinted that 6-OHG could regulate the

levels of genes associated with PI3K/AKT signaling pathway in the brain tissue of mice with HHBI. Previous studies also indicated that some structurally similar isoflavones, such as genistein,[23] daidzein,[24] formononetin,[25] and biochanin-A,[26] exhibited neuroprotective role by triggering the PI3K/AKT signaling pathway. Combined with transcriptome data in the present study and previous literature, it is speculated that the neuroprotection of 6-OHG against HHBI was attributed to the activation of PI3K/AKT signaling pathway.

To further investigate the involvement of the PI3K/AKT signaling pathway in 6-OHG-mediated protection against HHBI, we determined the expressions of p-PI3K and p-AKT, as only the phosphorylated forms of these proteins exhibit full enzymatic activity.[27] Western blot assays revealed that HH significantly downregulated the ratios of p-PI3K/ PI3K and p-AKT/AKT in brain tissue, indicating inhibition of the PI3K/AKT signaling pathway, which may participate in the pathogenesis of HHBI. In contrast, 6-OHG treatment considerably increased the ratios of p-PI3K/PI3K and p-AKT/AKT in brain tissue of mice with HHBI, suggesting that 6-OHG activates the PI3K/AKT signaling pathway. Molecular docking analysis demonstrated that 6-OHG has a strong binding ability with PI3K and AKT, further supporting its interaction with the PI3K/AKT pathway. Consistent with our expectations, the activation of this pathway by 6-OHG was effectively counteracted by LY294002, a well-characterized PI3K inhibitor extensively validated in brain injury models.[28,29] Meanwhile, the ameliorative effect of 6-OHG on the pathological change of brain tissue caused by HH was also negated by LY294002 treatment. These data indicate that 6-OHG mitigates HHBI via activating the PI3K/AKT signaling pathway.

Extensive evidence has indicated that oxidative stress was the key molecular mechanism underlying HHBI.[30–32] Under HH circumstances, hypoxia disrupts normal oxidative phosphorylation and impairs electron transport chain function, resulting in mitochondrial dysfunction and the excessive production of reactive oxygen species (ROS), causing an imbalance in redox equilibrium. Simultaneously, HH stimulation can destroy the antioxidant system, and further aggravate oxidative stress. Our previous report demonstrated that 6-OHG activates the Nrf2/HO-1 pathway, subsequently inhibiting oxidative stress induced by HH.[13] Nrf2, a downstream target of the PI3K/AKT pathway, has been shown to translocate to the nucleus upon PI3K/AKT activation, where it induces the expression of antioxidant enzymes. This process helps reduce ROS levels and restore redox balance.[33,34] In the present study, 6-OHG administration dramatically decreased H_2O_2 and MDA levels while restoring SOD activity and GSH content, compared with the HHBI group. Nevertheless, the anti-oxidative capacities of 6-OHG were partially intercepted when the PI3K/AKT pathway was inhibited by LY294002. These data suggest that 6-OHG mitigates HH-induced oxidative stress in brain tissue via activating the PI3K/AKT signaling pathway.

Inflammation also plays a significant role in mediating HHBI.[35] Our previous study demonstrated that 6-OHG modulates the NF-κB/NLRP3 pathway, thereby inhibiting inflammation caused by HH.[13] The PI3K/AKT pathway negatively regulates NF-κB, reducing neuroinflammation by suppressing the release of pro-inflammatory factors, including TNF-α, IL-1β, and IL-6.[36,37] Consistent with previous findings, we also observed that HH induced inflammatory responses, as evidenced by high contents of TNF-α, IL-1β, and IL-6, along with low level of IL-10. 6-OHG administration effectively reversed these alterations. Notably, its anti-inflammatory effects were effectively abrogated by co-treatment with the LY294002, suggesting that 6-OHG mitigates HH-induced neuroinflammation by stimulating the PI3K/AKT signaling pathway.

The PI3K/AKT signaling pathway is a well-established anti-apoptotic pathway that plays a significant role in recovery following CNS injury.[38,39] Upon activation, this pathway modulates apoptosis by regulating key effector molecules, including Bcl-2 and Bax.[40] Bax, a pro-apoptotic protein, and Bcl-2, an anti-apoptotic protein, are members of the Bcl-2 family, and the balance between their expression levels is critical in determining cell survival or apoptosis.[41] Additionally, caspase-9 acts as an initiator of apoptosis, while caspase-3 serves as an executioner,[42] and their expression levels are indicative of the extent of apoptosis.[43] In addition, mitochondria-endoplasmic reticulum crosstalk also plays a complementary role in apoptotic regulation.[44] Consistent with previous research,[13] in this study, we also observed that 6-OHG treatment dramatically decreased Bax expression, lowered the Bax/Bcl-2 ratio, and suppressed the activities of caspase-3 and −9 compared to the HHBI group. However, these anti-apoptotic effects of 6-OHG were notably blocked by LY294002, suggesting that 6-OHG inhibits neuronal apoptosis following HH exposure, through stimulation of the PI3K/AKT signaling pathway.

Conclusion

In summary, our study provided evidence that 6-OHG mitigates HHBI by suppressing oxidative stress, neuroinflammation, and apoptosis through initiation of the PI3K/AKT signaling pathways. These findings not only deepen our knowledge of the

protective mechanisms of 6-OHG but also offer novel ways for combating HHBI. At the same time, it also enhances the potential of 6-OHG as a novel drug for treating and preventing HHBI.

There were several limitations in this study. First, the transcriptome data did not reveal significant differences in the expression of PIK3CA and AKT1, two core genes related to PI3K/AKT signaling pathway, potentially due to the small sample size and inter-individual variability, which could obscure subtle but biologically relevant mRNA changes. Second, LY294002 has been demonstrated to be a valuable pharmacological tool for elucidating drug mechanisms through specific inhibition of the PI3K/AKT signaling pathway. However, it should be noted that LY294002 may exhibit off-target effects that complicate the interpretation of results. Therefore, future studies utilizing genetic knockout mouse models would provide more definitive evidence. Third, we used male mice that are more sensitive to the plateau environment in our study, but this can lead to gender bias, which may limit the generalizability of our findings to females. Fourth, while the PI3K/AKT signaling pathway has been proven to take part in mediating the protective effect of 6-OHG in this study, other signaling pathways, such as MAPK and RAS, may also be involved in the therapeutic efficacy of 6-OHG against HHBI based on the transcriptome data. Finally, our analysis focused on the whole brain rather than on distinct brain regions, which may exhibit differential response to HH stimulation. These issues will be resolved in further investigation.

Data Sharing Statement

RNA-Seq data have been deposited into the NCBI Gene Expression Omnibus (GEO) datasets under accession number (GSE307180). Full-length, uncropped Western blot images are provided in Supplementary Information. Raw biochemical assay data are available from the corresponding author upon reasonable request.

Ethics Statement

The animal study was approved by the Animal Care and Use Committee of 940th Hospital (No 2021KYLL241) and was conducted in strict accordance with the National Research Council's Guide for the Care and Use of Laboratory Animals.

Consent for Publication

All authors approved the final manuscript and the submission to this journal.

Funding

This work was supported by the National Natural Science Foundation of China (grant number 81872796) and the Institutional Foundation of The First Affiliated Hospital of Xi'an Jiaotong University (grant number 2022MS-11).

Disclosure

The authors declare no competing financial interests or personal relationships that could have influenced the work presented in this paper.

References

1. Wang YL, Li L, Paudel BR, Zhao JL. Genomic insights into high-altitude adaptation: a comparative analysis of Roscoea alpina and R. purpurea in the Himalayas. *Int J Mol Sci*. 2024;25(4). doi:10.3390/ijms25042265
2. Luks AM, Hackett PH. Medical conditions and high-altitude travel. *N Engl J Med*. 2022;386(4):364–373. doi:10.1056/NEJMra2104829
3. Marutani E, Morita M, Hirai S, et al. Sulfide catabolism ameliorates hypoxic brain injury. *Nat Commun*. 2021;12(1):3108. doi:10.1038/s41467-021-23363-x
4. Hou Y, Fan F, Xie N, et al. Rhodiola crenulata alleviates hypobaric hypoxia-induced brain injury by maintaining BBB integrity and balancing energy metabolism dysfunction. *Phytomedicine*. 2024;128:155529. doi:10.1016/j.phymed.2024.155529
5. Huang Y, Zhu S, Yao S, et al. Unraveling aging from transcriptomics. *Trends Genet*. 2025;41(3):218–235. doi:10.1016/j.tig.2024.09.006
6. Tian L, Zhao C, Yan Y, et al. Ceramide-1-phosphate alleviates high-altitude pulmonary edema by stabilizing circadian ARNTL-mediated mitochondrial dynamics. *J Adv Res*. 2024;60:75–92. doi:10.1016/j.jare.2023.07.008
7. Zeng Y, Cao W, Huang Y, et al. Huangqi Baihe Granules alleviate hypobaric hypoxia-induced acute lung injury in rats by suppressing oxidative stress and the TLR4/NF-κB/NLRP3 inflammatory pathway. *J Ethnopharmacol*. 2024;324:117765. doi:10.1016/j.jep.2024.117765
8. Chang TS. Isolation, bioactivity, and production of ortho-hydroxydaidzein and ortho-hydroxygenistein. *Int J Mol Sci*. 2014;15(4):5699–5716. doi:10.3390/ijms15045699
9. Tsuchihashi R, Kodera M, Sakamoto S, et al. Microbial transformation and bioactivation of isoflavones from Pueraria flowers by human intestinal bacterial strains. *J Nat Med*. 2009;63(3):254–260. doi:10.1007/s11418-009-0322-z

10. Zhang P, Zhang J, Tian Y, et al. Synthesis, antioxidant and anti-hypoxia activities of 6-hydroxygenistein and its methylated derivatives. *Zhong Nan Da Xue Xue Bao Yi Xue Ban*. 2024;49(2):236–246. doi:10.11817/j.issn.1672-7347.2024.230228
11. Chang T-S, Ding H-Y, Tai SS-K, Wu C-Y. Mushroom tyrosinase inhibitory effects of isoflavones isolated from soygerm koji fermented with Aspergillus oryzae BCRC 32288. *Food Chem*. 2007;105(4):1430–1438. doi:10.1016/j.foodchem.2007.05.019
12. Chen YC, Inaba M, Abe N, Hirota A. Antimutagenic activity of 8-hydroxyisoflavones and 6-hydroxydaidzein from soybean miso. *Biosci Biotechnol Biochem*. 2003;67(4):903–906. doi:10.1271/bbb.67.903
13. Shi Z, Zhang J, Ma H, Jing L. Network pharmacology and in vivo experimental studies reveal the protective effects of 6-hydroxygenistein against hypobaric hypoxia-induced brain injury. *Heliyon*. 2024;10(16):e36241. doi:10.1016/j.heliyon.2024.e36241
14. Shao J, Zhao T, Ma H-P, Jia Z-P, Jing -L-L. Synthesis, characterization, and antiradical activity of 6-hydroxygenistein. *Chem Nat Compd*. 2020;56(5):821–826. doi:10.1007/s10600-020-03161-5
15. Vlahos CJ, Matter WF, Hui KY, Brown RF. A specific inhibitor of phosphatidylinositol 3-kinase, 2-(4-morpholinyl)-8-phenyl-4H-1-benzopyran-4-one (LY294002). *J Biol Chem*. 1994;269(7):5241–5248. doi:10.1016/S0021-9258(17)37680-9
16. Yang C, Xin Y, Wang G, Ma H, Jing L. Protective mechanism of moslosooflavone against hypobaric hypoxia-induced brain injury: insights from network pharmacology and in vivo validation. *Eur J Pharmacol*. 2025;1004:178001. doi:10.1016/j.ejphar.2025.178001
17. Guo N, Wang X, Xu M, et al. PI3K/AKT signaling pathway: molecular mechanisms and therapeutic potential in depression. *Pharmacol Res*. 2024;206:107300. doi:10.1016/j.phrs.2024.107300
18. Xiong Y, Liang W, Wang X, et al. S100A8 knockdown activates the PI3K/AKT signaling pathway to inhibit microglial autophagy and improve cognitive impairment mediated by chronic sleep deprivation. *Int Immunopharmacol*. 2024;143(Pt 2):113375. doi:10.1016/j.intimp.2024.113375
19. Gong G, Yin L, Yuan L, et al. Ganglioside GM1 protects against high altitude cerebral edema in rats by suppressing the oxidative stress and inflammatory response via the PI3K/AKT-Nrf2 pathway. *Mol Immunol*. 2018;95:91–98. doi:10.1016/j.molimm.2018.02.001
20. Li N, Cheng Y, Jin T, et al. Kaempferol and ginsenoside Rg1 ameliorate acute hypobaric hypoxia induced lung injury based on network pharmacology analysis. *Toxicol Appl Pharmacol*. 2023;480:116742. doi:10.1016/j.taap.2023.116742
21. Wang N, Song J, Zhou G, Li W, Ma H. Mechanism of salidroside relieving the acute hypoxia-induced myocardial injury through the PI3K/Akt pathway. *Saudi J Biol Sci*. 2020;27(6):1533–1537. doi:10.1016/j.sjbs.2020.04.035
22. Ji L, Su S, Xin M, et al. Luteolin ameliorates hypoxia-induced pulmonary hypertension via regulating HIF-2α-Arg-NO axis and PI3K-AKT-eNOS-NO signaling pathway. *Phytomedicine*. 2022;104:154329. doi:10.1016/j.phymed.2022.154329
23. Guo J, Yang G, He Y, et al. Involvement of α7nAChR in the protective effects of genistein against β-amyloid-induced oxidative stress in neurons via a PI3K/Akt/Nrf2 pathway-related mechanism. *Cell Mol Neurobiol*. 2021;41(2):377–393. doi:10.1007/s10571-020-01009-8
24. Zhang F, Ru N, Shang ZH, et al. Daidzein ameliorates spinal cord ischemia/reperfusion injury-induced neurological function deficits in Sprague-Dawley rats through PI3K/Akt signaling pathway. *Exp Ther Med*. 2017;14(5):4878–4886. doi:10.3892/etm.2017.5166
25. Sugimoto M, Ko R, Goshima H, et al. Formononetin attenuates H(2)O(2)-induced cell death through decreasing ROS level by PI3K/Akt-Nrf2-activated antioxidant gene expression and suppressing MAPK-regulated apoptosis in neuronal SH-SY5Y cells. *Neurotoxicology*. 2021;85:186–200. doi:10.1016/j.neuro.2021.05.014
26. Singh L, Kaur N, Bhatti R. Neuroprotective potential of biochanin-A and review of the molecular mechanisms involved. *Mol Biol Rep*. 2023;50(6):5369–5378. doi:10.1007/s11033-023-08397-2
27. Chu N, Salguero AL, Liu AZ, et al. Akt kinase activation mechanisms revealed using protein semisynthesis. *Cell*. 2018;174(4):897–907.e814. doi:10.1016/j.cell.2018.07.003
28. Gu N, Yan J, Tang W, et al. Prevotella copri transplantation promotes neurorehabilitation in a mouse model of traumatic brain injury. *J Neuroinflammation*. 2024;21(1):147. doi:10.1186/s12974-024-03116-5
29. Li ZY, Yang X, Wang JK, et al. MFGE8 promotes adult hippocampal neurogenesis in rats following experimental subarachnoid hemorrhage via modifying the integrin β3/Akt signaling pathway. *Cell Death Discov*. 2024;10(1):359. doi:10.1038/s41420-024-02132-x
30. Maiti P, Singh SB, Sharma AK, et al. Hypobaric hypoxia induces oxidative stress in rat brain. *Neurochem Int*. 2006;49(8):709–716. doi:10.1016/j.neuint.2006.06.002
31. Li X, Zhang J, Liu G, et al. High altitude hypoxia and oxidative stress: the new hope brought by free radical scavengers. *Life Sci*. 2024;336:122319. doi:10.1016/j.lfs.2023.122319
32. Zhang J, Zhao T, Zhang P, et al. Moslosooflavone protects against brain injury induced by hypobaric hypoxic via suppressing oxidative stress, neuroinflammation, energy metabolism disorder, and apoptosis. *J Pharm Pharmacol*. 2024;76(1):44–56. doi:10.1093/jpp/rgad109
33. Liu Q, Jin Z, Xu Z, et al. Antioxidant effects of ginkgolides and bilobalide against cerebral ischemia injury by activating the Akt/Nrf2 pathway in vitro and in vivo. *Cell Stress Chaperones*. 2019;24(2):441–452. doi:10.1007/s12192-019-00977-1
34. Li J, Wang T, Liu P, et al. Hesperetin ameliorates hepatic oxidative stress and inflammation via the PI3K/AKT-Nrf2-ARE pathway in oleic acid-induced HepG2 cells and a rat model of high-fat diet-induced NAFLD. *Food Funct*. 2021;12(9):3898–3918. doi:10.1039/d0fo02736g
35. Zhou Y, Huang X, Zhao T, et al. Hypoxia augments LPS-induced inflammation and triggers high altitude cerebral edema in mice. *Brain Behav Immun*. 2017;64:266–275. doi:10.1016/j.bbi.2017.04.013
36. Chen S, Peng J, Sherchan P, et al. TREM2 activation attenuates neuroinflammation and neuronal apoptosis via PI3K/Akt pathway after intracerebral hemorrhage in mice. *J Neuroinflammation*. 2020;17(1):168. doi:10.1186/s12974-020-01853-x
37. Zhu Q, Enkhjargal B, Huang L, et al. Aggf1 attenuates neuroinflammation and BBB disruption via PI3K/Akt/NF-κB pathway after subarachnoid hemorrhage in rats. *J Neuroinflammation*. 2018;15(1):178. doi:10.1186/s12974-018-1211-8
38. Dudek H, Datta SR, Franke TF, et al. Regulation of neuronal survival by the serine-threonine protein kinase Akt. *Science*. 1997;275(5300):661–665. doi:10.1126/science.275.5300.661
39. Li L, Lin Z, Yuan J, et al. The neuroprotective mechanisms of naringenin: inhibition of apoptosis through the PI3K/AKT pathway after hypoxic-ischemic brain damage. *J Ethnopharmacol*. 2024;318(Pt A):116941. doi:10.1016/j.jep.2023.116941
40. Liu F, Hou Y, Chen X, et al. Moxibustion Promoted Axonal Regeneration and Improved Learning and Memory of Post-stroke Cognitive Impairment by Regulating PI3K/AKt and TACC3. *Neuroscience*. 2024;551:299–306. doi:10.1016/j.neuroscience.2024.05.027
41. Lan X, Wang Q, Liu Y, et al. Isoliquiritigenin alleviates cerebral ischemia-reperfusion injury by reducing oxidative stress and ameliorating mitochondrial dysfunction via activating the Nrf2 pathway. *Redox Biol*. 2024;77:103406. doi:10.1016/j.redox.2024.103406

42. Dehkordi MH, Munn RGK, Fearnhead HO. Non-canonical roles of apoptotic caspases in the nervous system. *Front Cell Dev Biol*. 2022;10:840023. doi:10.3389/fcell.2022.840023
43. Zhu R, Tong X, Du Y, et al. Improvement of chlorpyrifos-induced cognitive impairment by mountain grape anthocyanins based on PI3K/Akt signaling pathway. *Pestic Biochem Physiol*. 2024;205:106172. doi:10.1016/j.pestbp.2024.106172
44. Xie H, Tang J, Song L, et al. Mitochondria-endoplasmic reticulum crosstalk in apoptosis: the interactions of cytochrome c with monooxygenase and its reductase. *Int J Biol Macromol*. 2024;279(Pt 1):135160. doi:10.1016/j.ijbiomac.2024.135160